arXiv: 1601.01542

Astronomy & Astrophysics manuscript no. sanchezmenguiano2016
January 8, 2016

Shape of the oxygen abundance profiles in CALIFA face-on spiral galaxies

L. Sánchez-Menguiano[1,2], S. F. Sánchez[3], I. Pérez[2], R. García-Benito[1], B. Husemann[4], D. Mast[5,6], A. Mendoza[1], T. Ruiz-Lara[2], Y. Ascasibar[7,8], J. Bland-Hawthorn[9], O. Cavichia[10], A. I. Díaz[7,8], E. Florido[2], L. Galbany[11,12], R. M. Gónzalez Delgado[1], C. Kehrig[1], R. A. Marino[13,14], I. Márquez[1], J. Masegosa[1], J. Méndez-Abreu[15], M. Mollá[16], A. del Olmo[1], E. Pérez[1], P. Sánchez-Blázquez[7,8], V. Stanishev[17], C. J. Walcher[18], Á. R. López-Sánchez[19,20], and the CALIFA collaboration

ABSTRACT

We measured the gas abundance profiles in a sample of 122 face-on spiral galaxies observed by the CALIFA survey and included all spaxels whose line emission was consistent with star formation. This type of analysis allowed us to improve the statistics with respect to previous studies, and to properly estimate the oxygen distribution across the entire disc to a distance of up to 3-4 disc effective radii (r_e). We confirm the results obtained from classical H II region analysis. In addition to the general negative gradient, an outer flattening can be observed in the oxygen abundance radial profile. An inner drop is also found in some cases. There is a common abundance gradient between 0.5 and 2.0 r_e of $\alpha_{O/H} = -0.075\,\mathrm{dex}/r_e$ with a scatter of $\sigma = 0.016\,\mathrm{dex}/r_e$ when normalising the distances to the disc effective radius. By performing a set of Kolmogorov-Smirnov tests, we determined that this slope is independent of other galaxy properties, such as morphology, absolute magnitude, and the presence or absence of bars. In particular, barred galaxies do not seem to display shallower gradients, as predicted by numerical simulations. Interestingly, we find that most of the galaxies in the sample with reliable oxygen abundance values beyond ~ 2 effective radii (57 galaxies) present a flattening of the abundance gradient in these outer regions. This flattening is not associated with any morphological feature, which suggests that it is a common property of disc galaxies. Finally, we detect a drop or truncation of the abundance in the inner regions of 27 galaxies in the sample; this is only visible for the most massive galaxies.

Key words. Galaxies: abundances – Galaxies: evolution – Galaxies: ISM – Galaxies: spiral – Techniques: imaging spectroscopy – Techniques: spectroscopic

- Провели как попиксельный анализ данных обзора CALIFA, так и анализ HII областей.

- Критерии выборки:
  - Спиральные галактики Sa – Sm
  - Face-on (i<60)
  - Без признаков взаимодействия
  - H-alpha наблюдается на разных галактоцентрических расстояниях с S/N>4

- Отобрали 204 галактики, проанализировали из них – 129. В них – более чем 7100 областей HII.

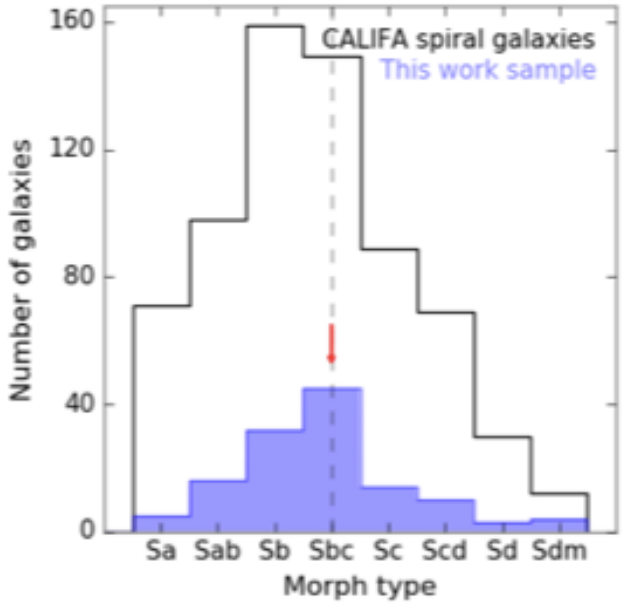

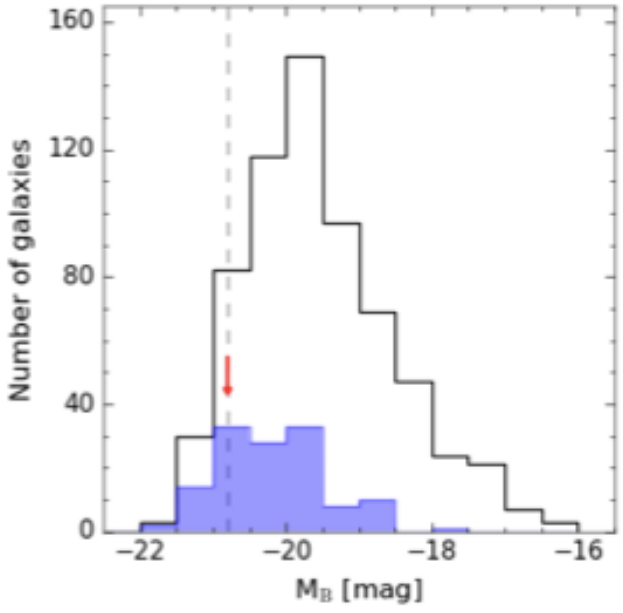

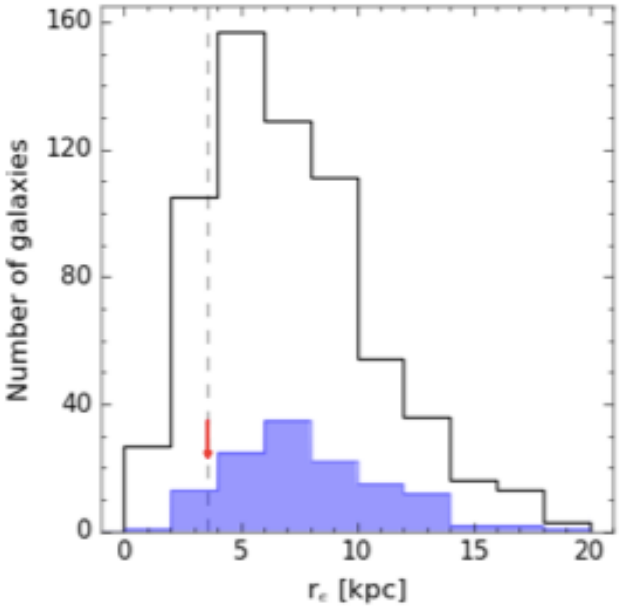

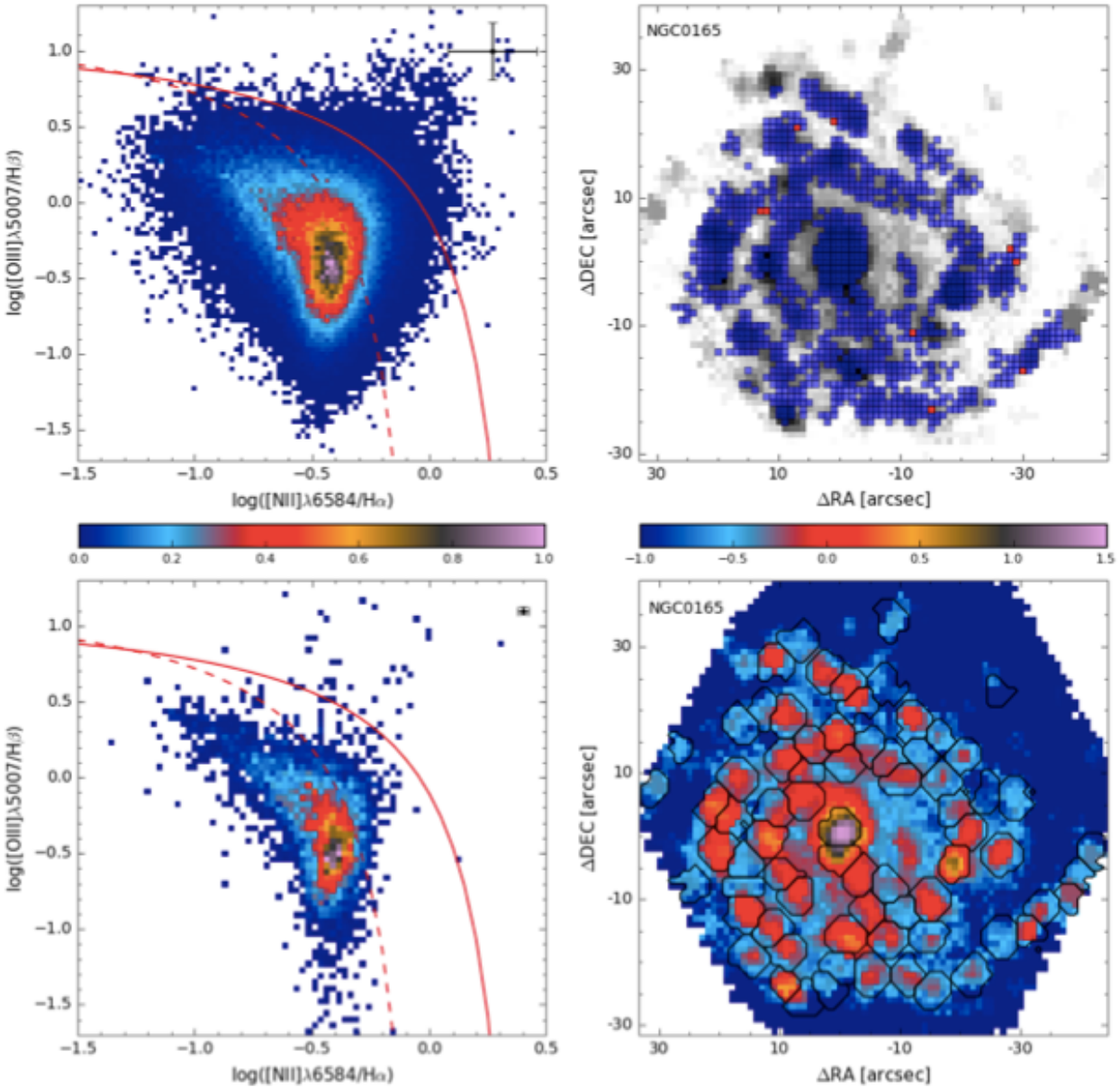

Fig. 3. *Left panels:* Normalised density distribution of the spaxels with EW(Hα) above 6 Å (top) and of the detected H II /SF regions (bottom) along the BPT diagram. The solid and dashed lines in both panels represent the Kewley et al. (2001) and Kauffmann et al. (2003) demarcation curves. SF regions are considered to be below the Kewley et al. (2001) curve. *Right panels:* Location of the spaxels classified as SF regions (blue dots) and AGNs (red dots) according to the BPT diagram superimposed on the IFS-based Hα map derived for one galaxy of the sample, NGC 0165 (top) and a Hα map in units of (log10) 10^{-16} erg s^{-1} cm^{-2} arcsec^{-1} for NGC 0165, together with the detected H II regions shown as black segmented contours (bottom).

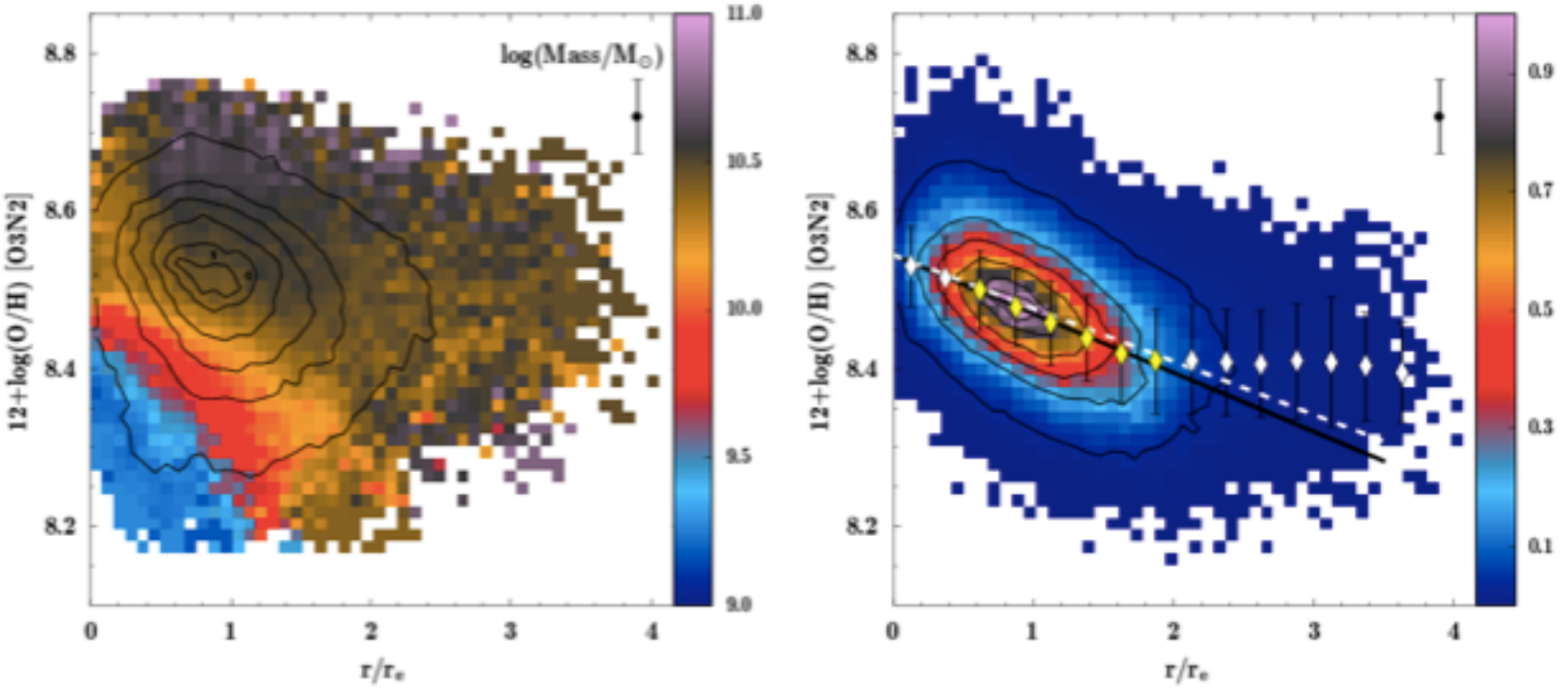

Fig. 8. *Left:* Radial distribution of the oxygen abundance derived using the O3N2 indicator and the calibration proposed by M13 for all the galaxies in our sample. The black contours show the density distribution of the star-forming spaxels, the outermost one including 95% of the total number of spaxels and decreasing 20% in each consecutive contour. The colour bar displays the average stellar mass of each galaxy (in log scale) corresponding to each abundance and radial distance. The average error of the derived oxygen abundances is indicated as an error bar located at the top right side of the panel. For clarity, only the oxygen abundance values with a contribution of at least 1% of the total number of spaxels are plotted. *Right:* Radial density distribution of the oxygen abundance after rescaling the oxygen abundances of each galaxy following the $\mathcal{M} - \mathcal{Z}$ relation derived in Sánchez et al. (2013). As in the left panel, the outermost contour encircles 95% of the total number of spaxels, decreasing 20% in each consecutive contour. The diamonds represent the mean oxygen abundance values, with the error bars indicating the corresponding standard deviations, for bins of 0.25 r_e. The solid-black line represents the error-weighted linear fit derived for those mean values within the range between 0.5 and 2.0 r_e (yellow diamonds), and the dashed white line represents the linear relation corresponding to the characteristic values of the zero-points and slopes derived in Sect. 4.1 for the individual galaxies assuming a Gaussian distribution for both parameters.

Универсальный градиент ~0.07 dex/re, если учесть зависимость Масса – Металличность.

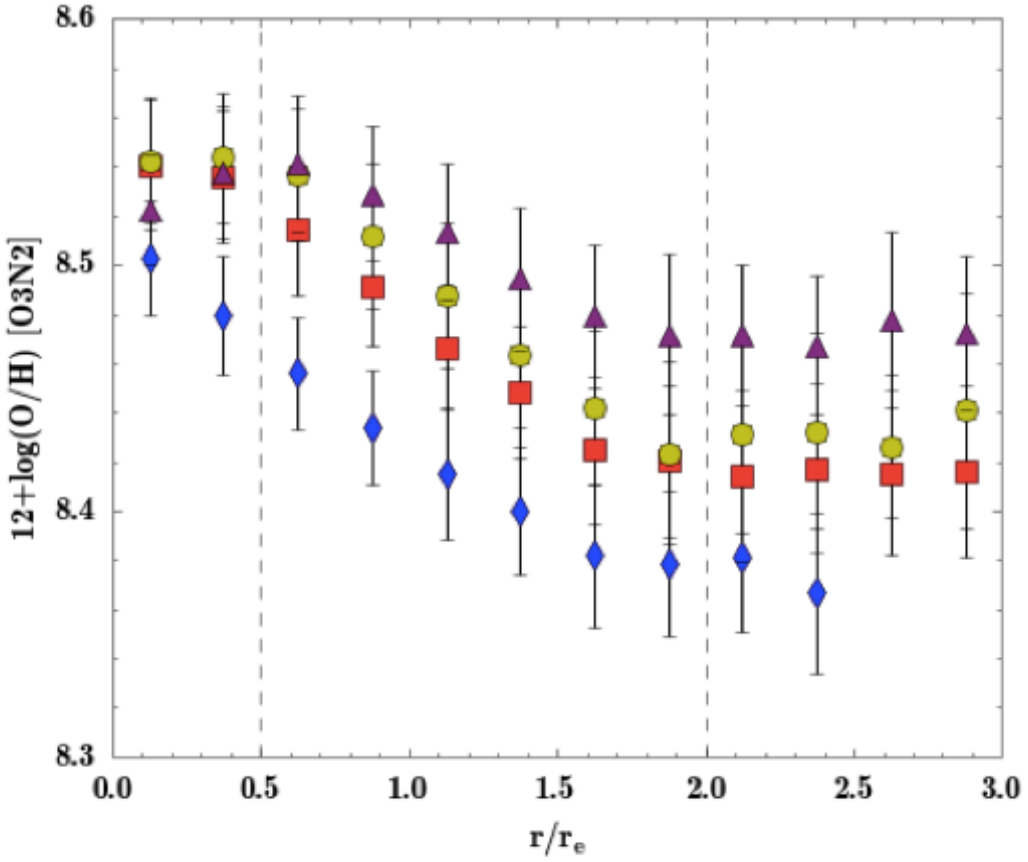

Fig. 9. Mean oxygen abundance radial profiles derived considering galaxies in four different bins according to their integrated stellar mass. The limits of the bins were chosen to ensure a similar number of elements in each bin: log ($M/M_\odot$) $\leq$ 10.2, blue diamonds; 10.2 $<$ log ($M/M_\odot$) $\leq$ 10.5, red squares; 10.5 $<$ log ($M/M_\odot$) $\leq$ 10.75, yellow dots; log ($M/M_\odot$) $\geq$ 10.75, purple triangles. The symbols represent the mean oxygen abundance values, with the error bars indicating the corresponding standard deviations, for bins of 0.25 r_e. Dashed vertical lines delimit the three different behaviours in the oxygen abundance profiles (i.e. drop in the inner parts, common gradient between 0.5 and 2.0 r_e, and the flattening in the outer parts).

Astrophysics and Space Science
DOI 10.1007/sXXXXX-XXX-XXXX-X

Chemical abundances in high-redshift galaxies: A powerful new emission line diagnostic

Michael A. Dopita[12], Lisa J. Kewley[13], Ralph S. Sutherland[3], & David C. Nicholls[1]

arXiv: 1601.01337

Abstract This *Letter* presents a new, remarkably simple diagnostic specifically designed to derive chemical abundances for high redshift galaxies. It uses only the Hα, [N II]and [S II] emission lines, which can usually be observed in a single gating stetting, and is almost linear up to an abundance of $12 + \log(\mathrm{O/H}) = 9.05$. It can be used over the full abundance range encountered in high redshift galaxies. By its use of emission lines located close together in wavelength, it is also independent of reddening. Our diagnostic depends critically on the calibration of the N/O ratio. However, by using realistic stellar atmospheres combined with the N/O vs. O/H abundance calibration derived locally from stars and H II regions, and allowing for the fact that high-redshift H II regions have both high ionisation parameters *and* high gas pressures, we find that the observations of high-redshift galaxies can be simply explained by the models without having to invoke arbitrary changes in N/O ratio, or the presence of unusual quantities of Wolf-Rayet stars in these galaxies.

- Предложен новый метод определения обилия кислорода по линиям H-alpha, [NII], [SII].
- Используемое соотношение потоков в этих линиях очень слабо зависит от ионизационного параметра и давления газа в ISM, практически линейно зависит от металличности

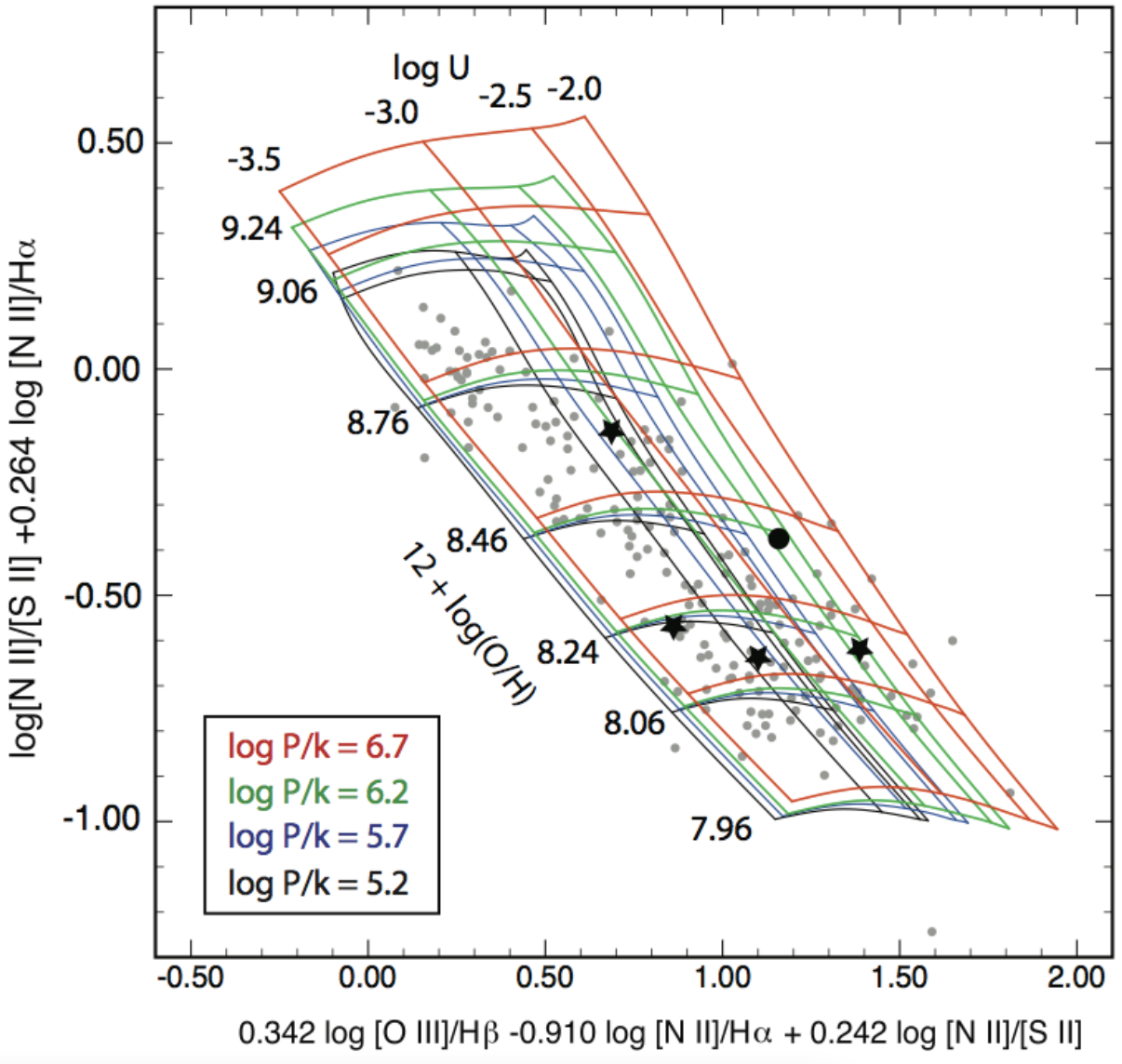

Fig. 2.— The 3D projection of the [N II]λ6484/Hα the [N II]λ6484/[S II]$\lambda\lambda$6717, 31 and the [O III]λ5007/Hβ line ratios which cleanly separates the abundance ($y-$axis) from the effects of pressure and ionisation pressure ($x-$axis). For comparison with the theoretical grid, the observations of van Zee et al. (1998) of individual H II regions in local spiral galaxies are shown as grey circles, and for high-redshift galaxies we plot the $z \sim 2$ MOSDEF stacks from Shapley et al. (2015) (stars), and the $z \sim 2$ composite spectrum from the Magellan FIRE survey from Masters et al. (2014) (filled black circle). These data points are generally consistent with sub-solar metallicity, high pressure, and high ionisation parameter.

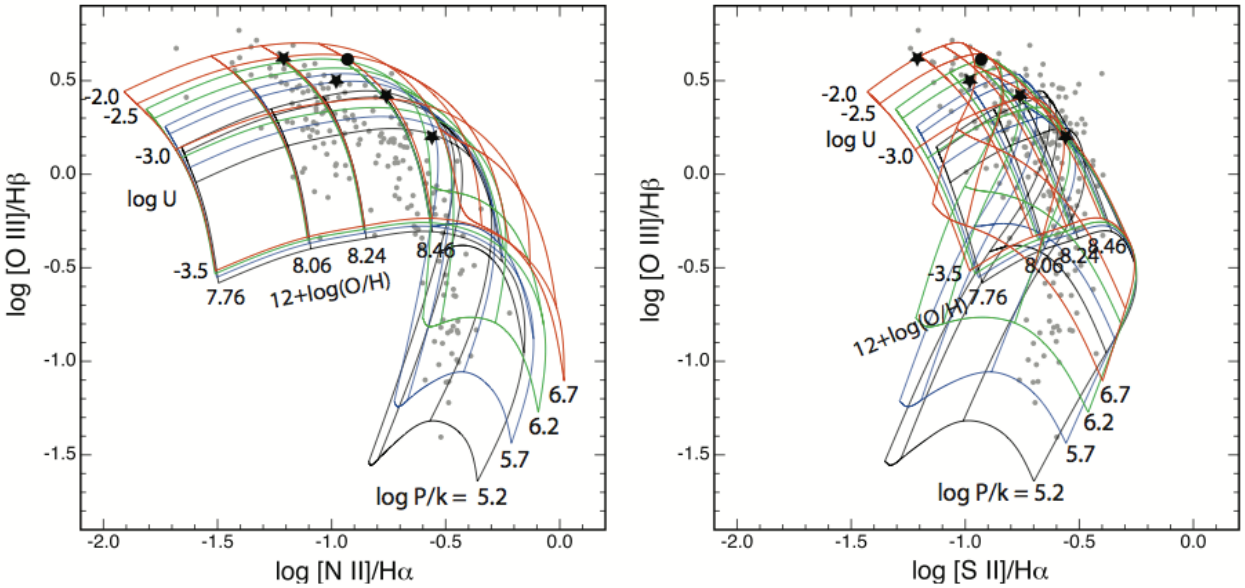

Fig. 4.— BPT diagrams showing the effect of pressure on the shape of the theoretical grids. The meaning of the symbols is the same as in Figure 2. For clarity, the values of $\log U$ are only marked for the case of the high-pressure grid. Note that a number of the van Zee et al. (1998) H II regions lie in the high pressure, high ionisation parameter regime, particularly those of lower abundance. Note also that the high-redshift galaxies are also consistent with having high pressure, high ionisation parameters and sub-solar metallicities in the H II region - in agreement with Figure 2. Clearly, there is no need to increase the relative N abundance in order to explain the high-redshift galaxy observations by Masters et al. (2014) and Shapley et al. (2015).

- Проблема: галактики на больших z показывают на BPT диаграммах повышенное отношение [OIII]/Hb при заданном [NII]/Ha. На зависимости [OIII]/Hb vs [SII]/Ha аналогичного разногласия с близкими галактиками не наблюдается.
- Ранее объяснялось возможным избытком WR звезд на больших z
- Впервые рассмотрели влияние давления ISM и построили соответствующие сетки моделей – показали, что наблюдаемое разногласие хорошо объясняется более высоким давлением в областях HII галактик на больших z.

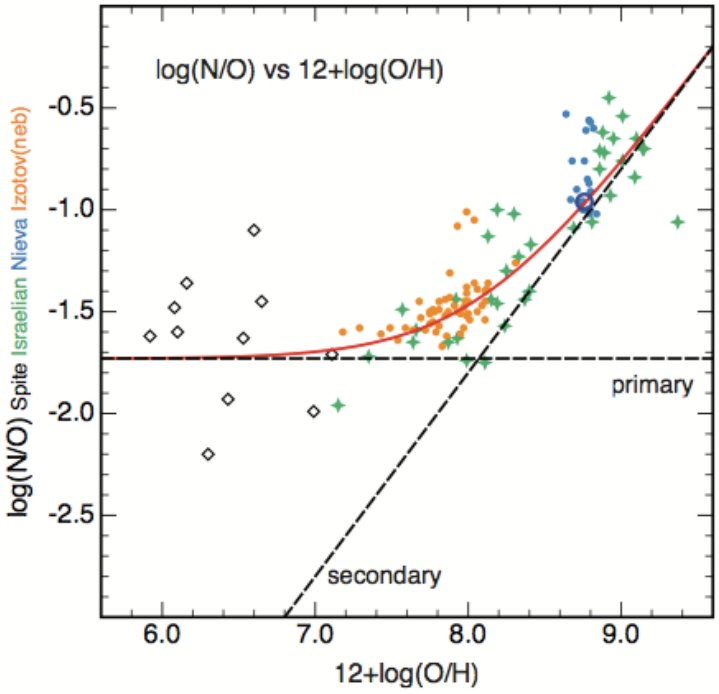

Fig. 1.— The calibration of N/O vs. O/H used in this paper. The data points are derived from the following papers: Izotov et al. (1999); Israelian et al. (2004); Spite et al. (2005) and Nieva & Przybilla (2012)

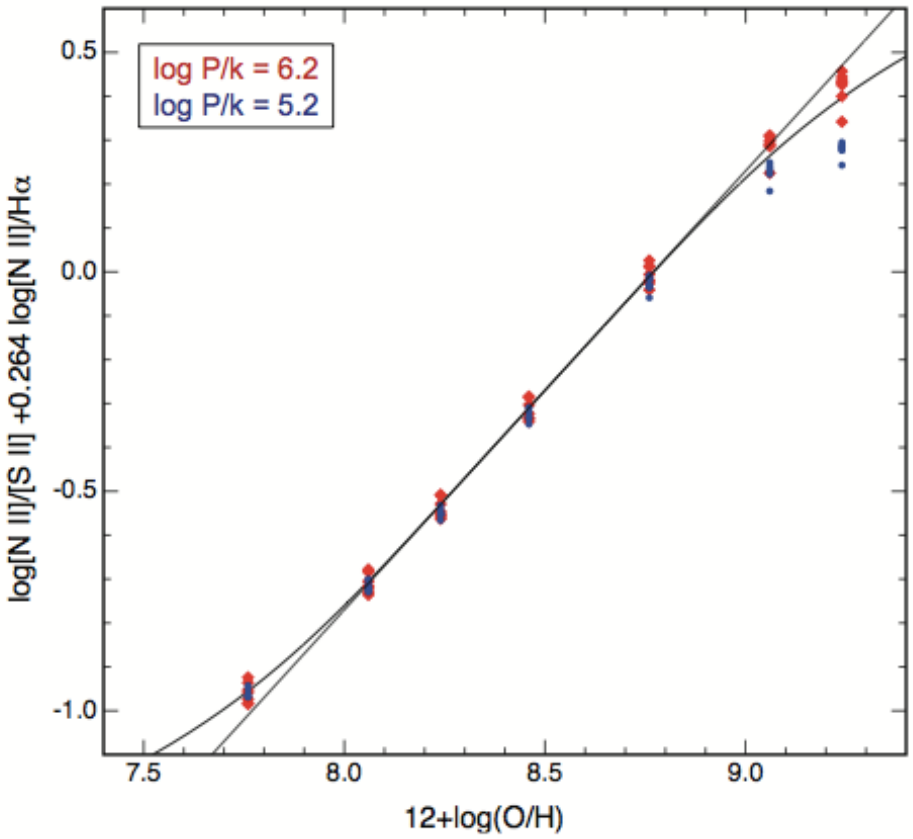

Fig. 3.— Calibration of the [N II]/[S II]and [N II]/Hα emission line ratio combination against $12 + \log(\mathrm{O/H})$. The red group of points represent the models having $\log P/k = 6.2\,\mathrm{cm}^{-3}\mathrm{K}$, while the blue points are for $\log P/k = 5.2\,\mathrm{cm}^{-3}\mathrm{K}$. The lines shown are the best linear fits and 5th. order fits as described in the text.

$$y = \log[\mathrm{NII}]/[\mathrm{SII}] + 0.264 \log[\mathrm{NII}]/\mathrm{H}\alpha, \quad (1)$$

$$12 + \log(\mathrm{O/H}) = 8.77 + y \quad (2)$$

$$12 + \log(\mathrm{O/H}) = 8.77 + y + 0.45(y + 0.3)^5, \quad (3)$$